Implications of ballast tank geometry and treatment technology on NIS removal

Zhixin Qi*, Ian Eames

University College London, Torrington Place, London WC1E 7JE, UK

Abstract

Regulation D-1 of the 2004 Ballast Water Management Convention requires that pumping seawater into a ballast tank should achieve a volumetric flushing efficiency of 95%. The IMO criteria for shipboard testing require a NIS removal rate of at least 90%. To examine the influence of tank geometry and treatment technology on satisfying IMO protocols, a general network model is developed and validated to analyse the transport of contaminants through a ballast tank.

The model is applied to analyse the flushing from typical ballast tanks. For the hopper side and upper wing tank considered, setting a single outlet further from the inlet may effectively improve the flushing efficiency. For the 'J'-type bottom and side tank considered, the flushing can be relaxed from 3 to 1.7 exchange volumes to save costs.

The influence of treatment technology on the NIS removal rate is investigated in the closed-loop system. For the 'J'-type tank considered, if the treatment efficiency is 70%, 2.4 times circulation is needed to achieve the 90% NIS removal rate.

Keywords:
ballast tank, ballast water, exchange volume, flushing efficiency, treatment efficiency, NIS removal

1. Introduction

Flow-through dilution of ballast water is a currently recommended and widely employed offshore method for controlling the introduction of NIS

---

*E-mail address: zhixin.qi.10@ucl.ac.uk
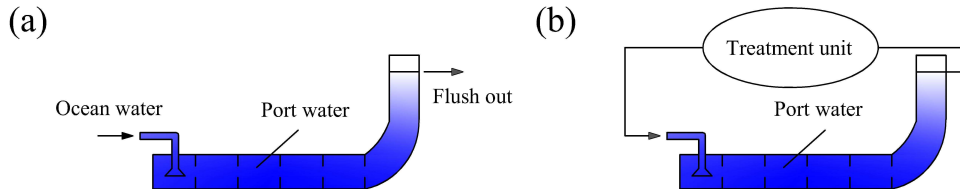
Fig. 1. Schematic of (a) a current open-loop ballast water flushing and (b) a future closed-loop treatment system.

(non-indigenous species) by ships (Murphy et al., 2004). NIS range from bacteria, plankton, fish eggs or crabs to fish, with a settling or swimming velocity, ranging from 0.1 to 150 mm/s. Many of the NIS are small and have densities comparable to water (e.g. bacteria, plankton, fish eggs), and can be considered passive. Large species, such as macroalgae, can survive and be transported in microscopic forms (Flagella et al., 2007). The IMO (International Maritime Organization, 2004) introduces specific legislation to reduce the potential for NIS being transported globally by ballast tanks. For ships employing the pumping-through method, Regulation D-1 of the 2004 Ballast Water Management (BWM) Convention requires that pumping open-ocean water into a full ballast tank should achieve a volumetric flushing efficiency ($\bar{C}$, defined as the fraction of the incoming water volume over the total water volume) of 95% and be carried out at least 200 nautical miles away from the mainland. Pumping three times the volume of ballast water tanks is considered to meet the standard; a reduction in the total number of exchange volumes is permitted providing the 95% flushing efficiency is established. The IMO requirements have put forward many technical challenges to ship design (Chen et al., 2013). The geometry of a ballast tank is rather complicated, even in most cases, the latitudinal and longitudinal section of a ballast tank are not symmetrical, which further increases the structural complexity (Eames et al., 2008).

Many ballast water treatment technologies have been proposed (see Table 1), including mechanical (filtration, cyclone), physical (ultraviolet, ultrasound, heat, etc.) and chemical (ozonation, chlorination, etc.) methods, according to different ship types (Endresen et al., 2004). The treatment efficiency (η) of the devices is defined as $\eta = (C_a - C_b)/C_a \times 100\%$, where C_a is the NIS concentration in the water before entering the treatment unit and C_b is the NIS concentration leaving the treatment unit, varying from

2

Table 1. Summary of ballast water treatment technologies.

Technology	Density effect	Treatment efficiency (η)
Filtration	no	30-90% (Parsons and Harkins, 2000)
Cyclone	no	60% (Waite et al., 2003)
Ultraviolet	no	40-100% (Champ, 2002)
Heat	yes	90-100% (Tsolaki and Diamadopoulos, 2010)
Ultrasound	no	40-100% (Gavand et al., 2007)
Chemicals	no	75-100% (Tsolaki and Diamadopoulos, 2010)

30% to 100%. Mamlook et al. (2007) performed a comparison among various proven ballast water treatment technologies aboard different types of ships, and found that filtration, ultraviolet and ultrasound are both effective and reliable; based on the benefit to cost ratio, filtration seems to provide the best combination of effective treatment and feasibility; meanwhile, radiolysis and chemical treatment are the least options, due to their high costs and low safety factors. Some of the treatment technologies do not change the density of the ballast water and their application requires understanding how fluid is flushed through a ballast tank. No current treatment option, however, can totally solve the NIS problem (Perakis and Yang, 2003), because none has been shown to be biologically effective, environmental friendly, economic, safe and practical at the same time (Goncalves and Gagnon, 2012). Due to underestimation of the technical challenges, insufficient resources and market economics (King et al., 2012), ballast water flushing will continue to be in widespread use for quite some time.

Some governments and authorities are now insisting on a combination of ballast water flushing and treatment. The Marine Environment Protection Committee adopted the 'Guidelines for ballast water exchange design and construction standards' in 2006, calling for special consideration on the feasibility of combining ballast exchange methods with treatment technologies

to meet the standards of Regulation D-2 of the 2004 BWM Convention, which requires the discharged ballast water containing less than 10 viable $\geq 50\mu$m organisms per m^3 and less than 10 viable $10 - 50\mu$m organisms per ml; and discharge of the indicator microbes shall not exceed the specified concentrations. According to the success criteria for shipboard testing - 2.2.2.5 of IMO Guidelines for approval of ballast water management systems (G8), the viable organism concentration of the ballast water to be treated should exceed 10 times the maximum permitted values in Regulation D-2.1. This indicates an equivalent NIS removal rate of at least 90% for shipboard testing (International Maritime Organization, 2008). In some cases, the efficiency of the treatment technologies varies below 90% for some kinds of organisms. For all but the largest ships, all the new technologies employed will use continuous flushing or recycling to clean the ballast water. In the current open-loop flushing system, seawater is continuously pumped to flush the ballast water out of the tank, shown in Fig. 1(a); in the closed-loop system consisting of a flushing unit and a treatment unit, ballast water is continuously cleaned and backflushed to the tank, shown in Fig. 1(b). The combined effect of using both flushing and treatment technology can be assessed by the NIS removal rate (R), defined as $R = (C_0 - C(t))/C_0 \times 100\%$, where C_0 is the original NIS average concentration of the ballast system and $C(t)$ is the NIS average concentration of the system varying with time. R measures the total removal of NIS from the whole system. Both the open-loop flushing and closed-loop treatment methodology require a general insight into the flushing efficiency.

Given that the bulk flushing efficiency of a ballast tank cannot be measured and only the water entering the tank is accessible, the main question is how the efficiency of the treatment plus the flushing process can be estimated. A number of methodologies can be applied to study the movement of NIS in a ballast tank, including field measurements, CFD (computational fluid dynamics), reduced models and small scale experiments. The advantages and disadvantages of these methodologies are listed in Table 2. Although field measurements are the most convincing, they tend to be expensive to undertake, be restricted to specific types and therefore cannot provide general laws for all kinds of ballast tanks. Single point measurements have been made of the tank discharge, but the uniformity of the initial dye concentration is unknown and the results are not general. CFD can provide detailed results, but the major challenge is the mesh quality for complex geometries; the meshing component may be a more significant task than the solve step. Reduced mathematical models are restricted to simple flows, but time saving

Table 2. Advantages and disadvantages of different methodologies for analysing flushing efficiency.

Methodologies	Advantages	Disadvantages
Field measurements	Valid	Expensive; Time consuming; Difficult to interpret
CFD	Detailed analysis; Whole field datasets	Difficult to validate; Unclear physical model
Reduced models	Time saving; Easy to extend	Restricted to simple flows; Restricted validity
Small scale experiments	Inexpensive; Easy to operate	Restricted validity

and easy to extend. The dimensionless groups characterizing small scale tests may not match those of field problems, which may restrict their applicability, but they tend to be easier to undertake.

The purpose of this paper is to examine the influence of tank design and treatment system on satisfying the IMO standards. This involves investigating how the NIS removal rate depends on ballast tank geometry, exchange volumes and treatment efficiency. Multizone network modelling has been used extensively in the context of analysing ventilation performance for moderately- and large-sized buildings (Chen, 2009; Chen et al., 2010). Li et al. (2008) and Parker and Bowman (2011) developed state-space models to predict contaminant transport in multizone systems. Zhao et al. (1998) evaluated the COMIS (Feustel and Smith, 1997) model by comparing simulation and measurement of airflow and pollutant concentration. This technique has not been applied to study flushing from ballast tanks. Most multizone models are built up from simple network models for connectivity and empirical rules for resistance. A critical element of these models is their validation by comparison with detailed experiments that exhibit a degree of complexity similar to the practical case. In Section 2, how the mathematical model is

set up for multizone flow is described. In Section 3, the multizone model is validated by comparison with a series of laboratory experiments in much more detail, which test the hole resistance and compartment division of a four compartment tank. The model is then applied to analyse flushing typical ballast tanks of the open-loop system in Section 4. In Section 5, the influence of treatment technology on the NIS removal rate is analysed in the closed system. In Section 6, the main results are summarised and conclusion is made.

2. Mathematical model of multizone flow

A multizone model typically represents compartments to a tank as nodes to a network, as illustrated in Fig. 2(a), which may lie at different heights. To use an electrical analogy, the inhomogeneity in the system is through varying capacitors and resistors. Each node (denoted by i) is characterised by a capacitance (or volume, V_i). The connection between the nodes represent the flow pathways and these are characterised by a resistance (pressure drop coefficient, $\zeta_{i,j}$). In ballast tanks, capacitance and resistance correspond to different volume of compartments and size/shape of connecting passages.

Focussing on the generality of the formulation, the flow through the network is driven by volumetric sources at the inlet. Ballast water flushing is normally characterised by a high level of turbulence due to the sharp edges in the lightening frames between compartments in ballast tanks. The assumption of uniform density is appropriate especially since the ballast water is taken 12 m below the water surface on cargo tankers, similarly for seawater ports such as Singapore. In the case of proposed treatment technologies such as ultraviolet and ultrasound, which are applied in transit, the density difference between re-injected (cleaner) water and ballast water can be neglected. As such, stratification effects tend to be weak. The extent of fluid mixing depends on Reynolds number. In typical ballast tanks, the Reynolds number is $10^4 \sim 10^6$, so the highly turbulent flow can be assumed to mix perfectly within each compartment (Qi et al., 2014). Small species in ballast water are essentially advected with the flow and can be regarded as essentially passive during flushing.

Fig. 2(b) shows a schematic of a node within the network. p_i is the pressure of the centre of node i. The volume flux from node i to its neighbouring
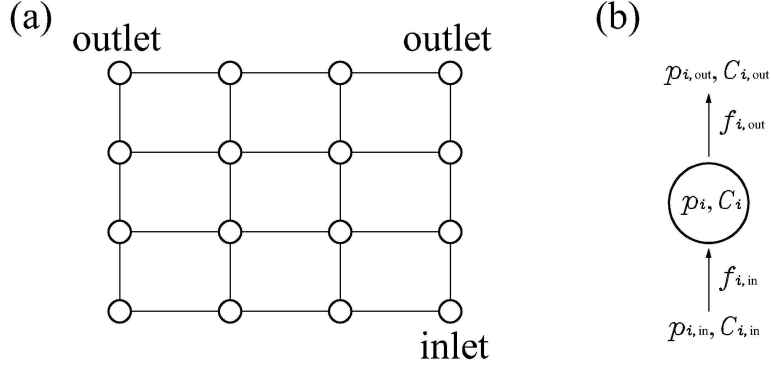
Fig. 2. Schematic of a (a) network and (b) node i with notations of pressure (p_i) and flushing efficiency (C_i). The volume flux from node i to node j is denoted by $f_{i,j}$.

node j through a hole with cross sectional area $A_{i,j}$ is defined as

$$f_{i,j} = \int_{A_{i,j}} \boldsymbol{u} \cdot \hat{\boldsymbol{n}} \mathrm{d}A, \tag{1}$$

where $\boldsymbol{u}$ is the velocity field and $\hat{\boldsymbol{n}}$ is a unit normal vector directed from node i to node j. The flushing efficiency in node i (of volume V_i), C_i, is defined as the fraction of the incoming fluid over the total fluid in the node.

A system of ordinary differential equations is developed by integrating over individual nodes. The inertial force of the fluid is sufficiently large when compared to the buoyancy force that the latter can be ignored. The basis of the model is that the incoming matter is well mixed and p is the same within each node, but the gradients of p and C are large between nodes. Integrating the continuity equation over node i and substituting into (1) gives

$$\sum f_{i,\mathrm{in}} - \sum f_{i,\mathrm{out}} = 0, \tag{2}$$

where $f_{i,\mathrm{in}}$ and $f_{i,\mathrm{out}}$ are the volume inflow and outflow rates respectively.

For steady flows, the multizone model of flow between nodes employs a closure model to relate the pressure drop with the average velocity through the holes. The pressure difference between two neighbouring nodes i and j is

$$p_i - p_j = \zeta_{i,j} \rho \frac{|f_{i,j}| f_{i,j}}{A_{i,j}^2}. \tag{3}$$

Here $\zeta_{i,j}$ is the local pressure loss coefficient between nodes i and j. The pressure loss coefficient ζ is usually determined empirically. Different forms of the closure have been developed to account for windows, doors and sharp openings in a circular pipe. At high Reynolds numbers, Heiselberg et al. (2001) and Chu et al. (2010) found that ζ depends primarily on the ratio (β) of the hole area to the partition wall area. For square openings between rooms, Chu and Wang (2010) found that ζ increases rapidly with β when $0 \leq \beta \leq 5\%$. Meizig and Schmidt (1965) found that ζ increases approximately linearly with $\sqrt{\beta}$ for $5\% \leq \beta \leq 50\%$. Typically, $\beta \leq 20\%$ for ballast tanks. To close the pressure drop coefficient of an opening between two neighbouring compartments in this study ($3.27\% \leq \beta \leq 29.4\%$), a square root fit is used based on the results of Meizig and Schmidt (1965),

$$\zeta = 4.24\sqrt{\beta}, \tag{4}$$

for $0 \leq \beta \leq 50\%$.

The fluid is transported by the mean flow velocity and mixed by turbulent dispersion. The mean velocity is largest in the passage between compartments and is smallest within compartments. The sharp edge of the hole between compartments means that vortex shedding occurs and in this class of flows, the level of turbulence is comparable to the mean flow velocity. In the gap, a straining flow leads to a suppressing of the turbulence. Consequently the fluid tends to be rapidly mixed within a compartment. Thus an approximate model is used to describe the variation of the flushing efficiency in node i with time,

$$V_i \frac{dC_i}{dt} = \sum f_{i,\text{in}} C_{i,\text{in}} - \sum f_{i,\text{out}} C_i. \tag{5}$$

C_i is calculated as a function of dimensionless time T, based on flushing the total volume of the system (V), i.e.,

$$T = \frac{Qt}{V}, \tag{6}$$

where $T = 0$ corresponds to the network starting to be flushed. T can be interpreted as 'exchange volumes'. The average flushing efficiency of the NIS within the whole network, $\bar{C}$, is defined as

$$\bar{C} = \frac{\sum_i C_i V_i}{V}. \tag{7}$$

8

3. Model validation

Validating the mathematical model is crucial to have some faith in the fidelity of the predictions. The gold standard is to validate against experimental results, over a variety of parameters. To maintain a high degree of complexity but reduce the number of variables, the model was chosen to be a four node network, because it is analytically tractable. Fig. 3 shows a schematic of a four node inhomogeneous network, which physically corresponds to a tank with four interconnected compartments, denoted as 1, 2, 3 and 4. The inlet to the network is node 1, while two outlets are node 3 and 4. $k_1 L$ and $k_2 W$ are used to represent the length and width of compartment 1, where the tank has length L and width W. To validate the four elements of the model described in Section 2, the following tests were considered:

(1) varying the size of the interconnecting holes to generate inhomogeneous resistance for fixed capacitance;

(2) varying the size of the compartments to generate inhomogeneous capacitance for fixed resistance;

(3) examining the influence of flux constrained outlets versus pressure controlled outflow;

(4) examining the flushing efficiency of a passive contaminant through the system with steady release of dye to a node.

3.1. Model predictions

Different outlet arrangements are considered to investigate different flow allocation, corresponding to (a) volume flux constrained (one outlet at node 4 or 3) and (b) pressure constrained (two outlets at node 3 and 4). These are referred to as (a) 'far/near open' and (b) 'both open'. The modelling is shown in Appendix A.

The test cases (1-4) described at the start of Section 3 are analysed using the following constraints to the model:

(1) fixed capacitance, $k_1 = k_2 = 1/2$, and varying ϕ ($\phi = f_{1,2}/Q$, see Appendix A);

(2) fixed resistance, $\zeta_{1,2} = \zeta_{2,4} = \zeta_{1,3} = \zeta_{3,4}$, and varying k_1, k_2;

9
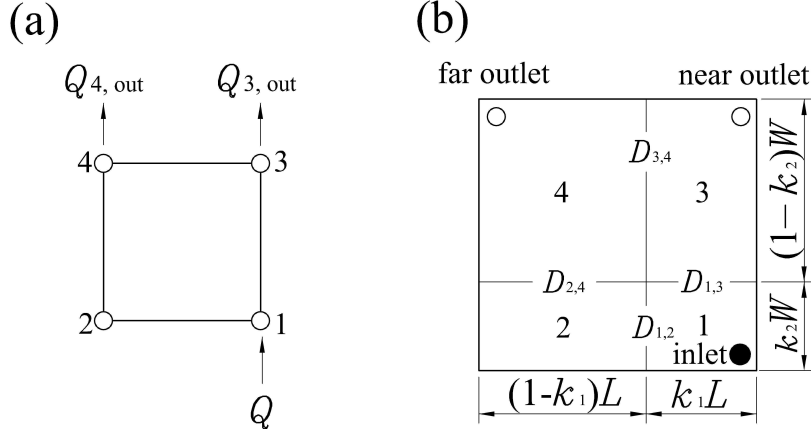
Fig. 3. A four node mesh network with one inlet and two outlets. D is the diameter of the hole between neighbouring compartments; $k_1 L$ and $(1-k_1)L$ are the length of compartment 1 and 2 respectively; $k_2 W$ and $(1-k_2)W$ are the width of compartment 1 and 3 respectively.

(3) flux constrained ($Q_{4,\text{out}} = Q$ corresponding to 'far open' or $Q_{3,\text{out}} = Q$ corresponding to 'near open') or pressure controlled ($p_3 = p_4 = 0$ corresponding to 'both open') - see Table A1;

(4) constant Q, $C = 1$ on inlet and $C = 0$ at $T = 0$ in the tank.

3.2. Experimental methodology and errors

A square clear acrylic tank of width 61 cm and height 20 cm was used in the experimental study (see Fig. 4(a) and (b)). Two large rectangular plates were used to generate the four internal configurations in the tank (see the bottom of Fig. 4(c)). The two plates were crossed each other in the middle and inserted into the tank (see Fig. 4(a)). The flow resistance between two neighbouring compartments were varied by inserting small plates with different sizes of circular holes ($D = 5$, 10 or 15 cm, see Fig. 4(c)). To change the capacitance for the four compartments in the tank, two large plates of the same dimension, but with three circular holes each, were employed (see Fig. 4(d)). Different combinations of two of the four large plates can set k_1 and k_2 to be 1/3, 1/2 or 2/3. Three valved pipes were inserted through the top cover into the tank as potential inlets, and three valved pipes on the opposite side as potential outlets. The inflow rate was fixed at $Q = 0.25$ l/s

10
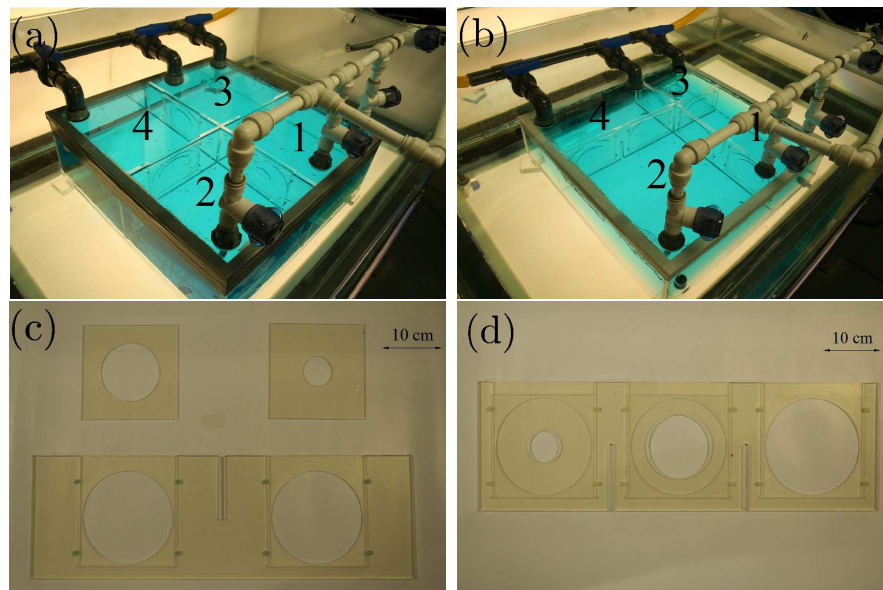
Fig. 4. Photograph of a configuration of (a) inhomogeneous hole resistance and (b) inhomogeneous compartment division of the four compartment tank, (c) two one-hole plates (16 cm × 18 cm × 0.5 cm) and a two-hole plate (61 cm × 20 cm × 1 cm), and (d) a three-hole plate (61 cm × 20 cm × 1 cm) used in the experimental study.

(see test(4)). The Reynolds number (defined as $Re = UD/\nu$, where U is the average flow velocity through the inlet, D the diameter of the inlet hole and ν the kinematic viscosity of water.) at the nozzle exit was $Re_n \sim 8000$. To test the influence of boundary conditions (test (3)), three outlet arrangements were considered: 'far open', 'near open', and 'both open', corresponding to flux and pressure constraints; these are described in Table A1.

The acrylic model was illuminated by a uniform diffuse light source placed beneath; an inclined mirror was placed above the tank to obtain the plan view. At the start of each experiment, the tank was filled with clear water (i.e. $C = 0$ at $t = 0$), and a dilute methylene blue dye solution (concentration of 0.1 mg/l) was pumped into the tank via the inlet. Images were taken at a rate of 7.5 frames per second by an Allied Vision Dolphin machine vision camera. Each compartment within the tank was individually masked and analysed so that the time series of the total mass of dye in each compartment could be evaluated by Matlab Image Processing Toolbox. An optical method was used to assess the mass of dye within each compartment based on classical absorption theory of Lambert-Beer (Cenedese and Dalziel, 1998). The image processing was based on the principle that the depth integrated dye concentration at a point can be related to the reduction of light intensity observed by the camera.

The major experimental measurement errors are caused by masking and calibration. From a series of calibration tests, a standard error of $\pm 2\%$ was observed in relating dye concentration to light intensity. On the top and bottom of the tank, lack of transparency in some points may decrease the measured dye concentration by about 1%. The compartments of the tank are individually assessed by masking part of the total image. The compartments had dimensions of around 100×100 pixels; masking is accurate to within 10 pixels and thus gives an error of 1%. During the pumping and flushing, small bubbles attached to the wall that form due to temperature change inside the tank may lead to a maximum error of 1%. In total, the experimental measurements have an error less than 5%. More systematic errors occur for the multiple outlets ('both open') configuration because of the difficulty of setting the pressure on the two outlets to be equal.

3.3. Model validation

In this section, the experimental results are compared with the theoretical predictions of C_i (for i=1, 2, 3, 4). The single outlet cases are flux constrained, and the double outlets case is pressure constrained. Fig. 5 and

6 show the influence of varying resistance and capacitance, respectively. For the case of varying resistance, the diameter of the connecting holes are explicitly shown in Fig. 5(a), (c) and (e). In general, the inhomogeneous resistance is characterised by ϕ (see Table A1), which differs depending on whether the flow is flux or pressure constrained. For the case of varying capacitance, the ratios of the length and width of each compartment are shown in Fig. 6, and the capacitance characterised by k_1 and k_2. In Fig. 5(a), (c) and (e) and Fig. 6, the time dependent flushing efficiency of each compartment is followed in time, while the influence of the inhomogeneous resistance and capacitance for $T = 1$ and $T = 3$ is shown in Fig. 5(b), (d) and (f) and Table 3.

3.3.1. Varying resistance

This case corresponds to test (1). The capacitance of the compartments was kept constant by fixing the volume of the compartments at $k_1 = k_2 = 1/2$. Fig. 5 shows a comparison between experimental measurements and theoretical predictions of C_i against T in (a), (c) and (e) and $\bar{C}$ against ϕ at $T = 1$ and $T = 3$ in (b), (d) and (f).

For the 'far open' case (Fig. 5(a)), the resistance of the flow pathway $1 \rightarrow 2 \rightarrow 4$ is lower than $1 \rightarrow 3 \rightarrow 4$ (at $\phi = 0.74$), leading to $C_2 > C_3$. The experimental measurements agreed well with the model predictions, although C_3 and C_4 were a little higher than estimated initially. From Fig. 5(b), it can be seen that $\bar{C}$ reaches the maximum value when $\phi = 0.5$; as expected $\bar{C}$ has a symmetric dependence on ϕ around $\phi = 0.5$. As $\phi = 0$ or 1, $\bar{C}|_{T=3} \approx 0.75$ because only three of the four compartments are flushed. As $\phi = 0$, $\bar{C}|_{T=3}$ was underestimated in practice because of the existence of fluid exchange between compartments 4 and 2 as $C_4 \gg C_2$ after the tank had been flushed for a long time.

For the 'near open' case (Fig. 5(c)), the resistance of the flow pathway $1 \rightarrow 3$ is much lower than $1 \rightarrow 2 \rightarrow 4 \rightarrow 3$ (at $\phi = 0.17$), leading to C_1 and C_3 being evacuated faster than C_2 and C_4. The main character of the flushing was predicted well by the model. From Fig. 5(d), it can be seen that $\bar{C}$ increases with ϕ. At $\phi = 0$, $\bar{C}|_{T=3} \approx 0.5$, as only compartments 1 and 3 are flushed; at $\phi = 1$, the four compartments are flushed through $1 \rightarrow 2 \rightarrow 4 \rightarrow 3$ and $\bar{C}|_{T=3} \approx 1$. That means that a linear network, or in graph theory, a Hamiltonian path (Montalbano, 1962), is the best flushing strategy. At $\phi = 0$, $\bar{C}$ was underestimated by the model due to the fluid exchange between compartments 3 and 4.

For the 'both open' case (Fig. 5(e)), C_2 is flushed faster than C_3 because
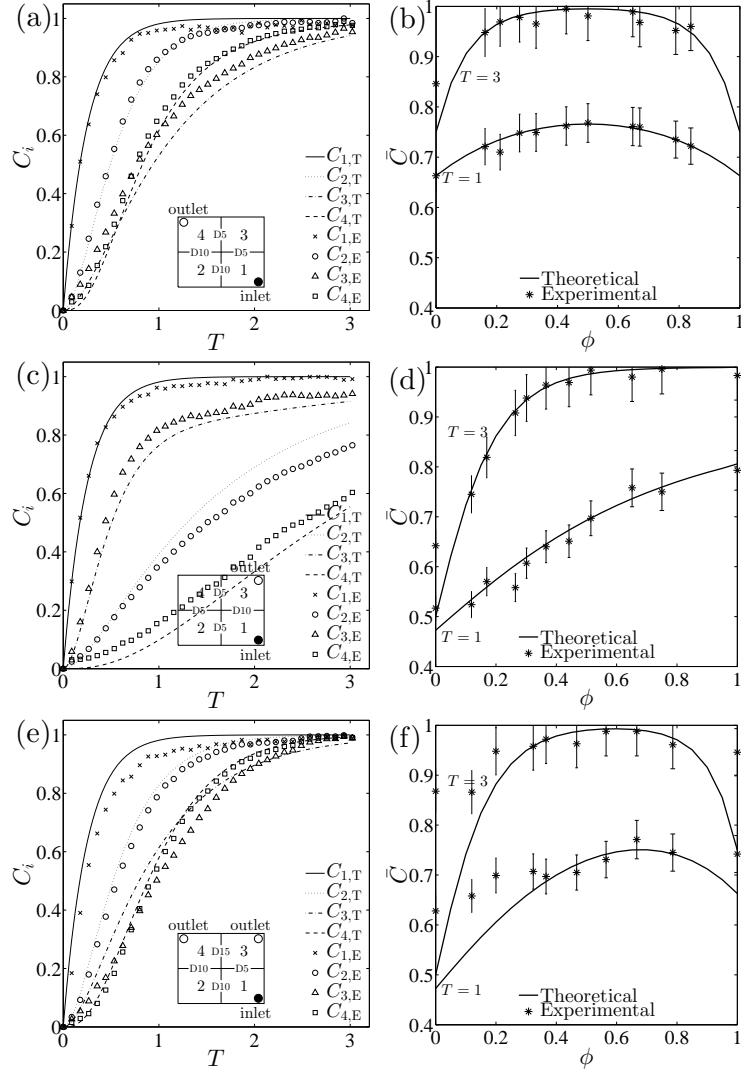
Fig. 5. The variation of C_i against T is shown in (a), (c) and (e), and $\bar{C}$ against ϕ at $T = 1$ and $T = 3$ is shown in (b), (d) and (f) for the four node network. In (a), (c) and (e), '$C_{i,\mathrm{T}}$' represents theoretical predictions, while '$C_{i,\mathrm{E}}$' represents experimental measurements; the diameters of the connecting holes are shown on the schematic. The figures correspond to (a, b) 'far open', (c, d) 'near open' and (e, f) 'both open' cases.

14

the resistance of the flow pathway $1 \to 2 \to 4$ is smaller than $1 \to 3$ (at $\phi = 0.67$). From Fig. 5(f), $\bar{C}$ reaches the maximum value at $\phi \approx 2/3$. When $\phi = 0$, $\bar{C}|_{T=3} \approx 0.5$, as only compartments 1 and 3 are flushed; at $\phi = 1$, $\bar{C}|_{T=3} \approx 0.75$, as only compartments 1, 2 and 4 are flushed. The discrepancy between the theoretical predictions and the experimental results is caused by the assumption that there is no flow between compartments 3 and 4 while the pressure difference between compartments 3 and 4 cannot be ignored in reality. It can be inferred that if the network cannot be made linear, the best strategy for flushing is to keep the flow allocation to one pathway approximately equal to the ratio of the volume that is to be flushed on this way. There are significant challenges to keep $\Delta p = 0$.

The agreement between experiments and the theory is good except for the pressure constrained case and large differences in resistance (i.e. when $\phi < 0.2$ or > 0.9), because the fluid exchange between compartments 3 and 4 cannot be completely ignored in these cases. This difference is largely attributed to the difficulty of maintaining the same pressure in compartments 3 and 4.

3.3.2. Varying capacitance

This case corresponds to test (2). The resistance between the nodes is fixed. The capacitance of this tank is determined by two parameters k_1, k_2 (Because of the way the resistance measure is defined ϕ is different in the example, see Table A1.). The comparison between experiments and predictions of the variation of C_i in the four node network is shown in Fig. 6. For the 'far open' case, $\phi = 1/(1 + ((k_2^{-1/2} + (1 - k_1)^{-1/2})/(k_1^{-1/2} + (1 - k_2)^{-1/2}))^{1/2})$ (see Table A1). When $k_1 = k_2 = 1/3$ (Fig. 6(a)), by symmetry $C_2 = C_3$ and this is confirmed experimentally. C_4 increases the most slowly because compartment 4 is the last compartment (and largest) to be flushed. When $k_1 = 2/3$, $k_2 = 1/3$ (Fig. 6(b)), $C_2 > C_3$ because although $f_{1,2} = f_{1,3}$, as a result of $V_2 < V_3$, C_2 increases faster than C_3. Originally, $C_3 > C_4$ as compartment 3 is directly flushed by compartment 1; at a later stage, compartment 2 has been sufficiently flushed so that C_2 is high and contributes a lot to the increment of C_4. The experimental results supported the theoretical predictions, although the theory does not consider the impact of the compartment size on the flow resistance. This means that the pressure drop of the fluid flow in the tank was mainly caused by contraction of the flow area due to existence of the holes between compartments, rather than the flow friction within compartments.
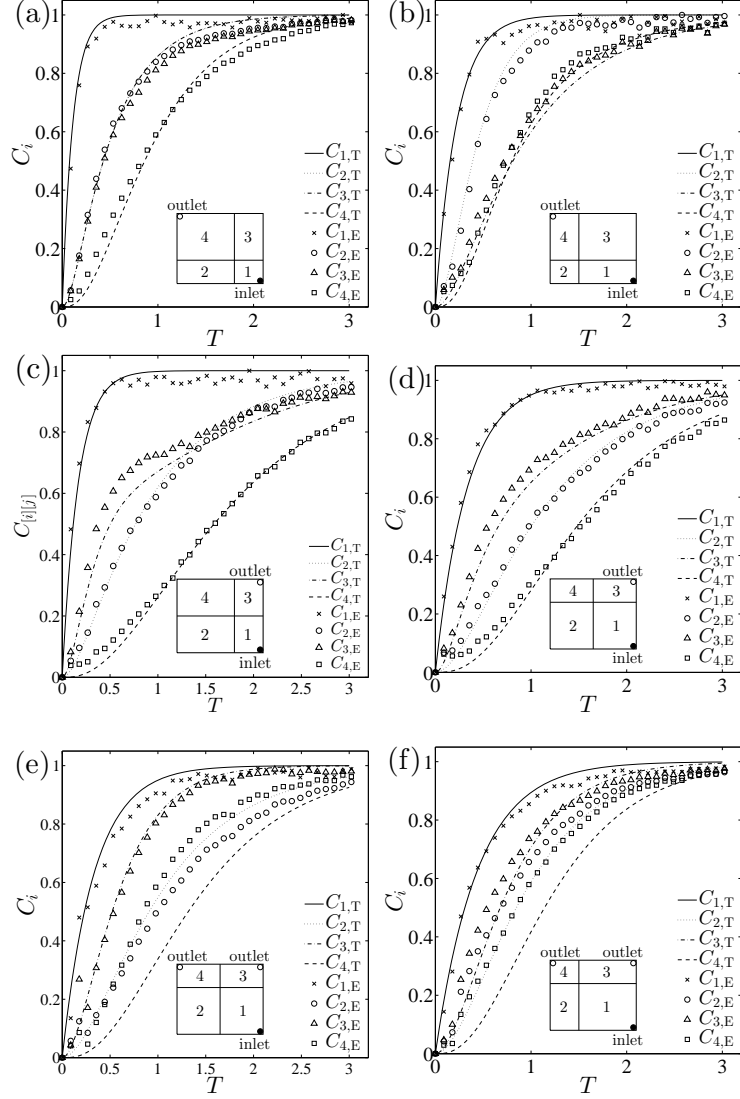
Fig. 6. C_i against T in the four node network for different compartment volumes. '$C_{i,\mathrm{T}}$' represents theoretical predictions, while '$C_{i,\mathrm{E}}$' represents experimental measurements. The figures correspond to (a, b) 'far open', (c, d) 'near open' and (e, f) 'both open' cases; (a) $k_1 = k_2 = 1/3$, (b) $k_1 = 2/3$, $k_2 = 1/3$, (c) $k_1 = 1/3$, $k_2 = 1/2$, (d, e) $k_1 = 1/2$, $k_2 = 2/3$, (f) $k_1 = k_2 = 2/3$.

16

Table 3. Flushing efficiency at $T = 1$ and $T = 3$ with different combinations of k_1 and k_2 in the four node network.

		Theoretical/experimental flushing efficiency (%)					
		Far open		Near open		Both open	
k_1	k_2	$T = 1$	$T = 3$	$T = 1$	$T = 3$	$T = 1$	$T = 3$
1/3	1/3	75.5/74.1	99.4/97.5	56.7/53.4	91.5/89.5	64.0/64.7	94.7/92.7
1/3	1/2	75.4/72.7	99.1/98.3	57.2/57.4	92.5/91.2	64.4/64.1	95.6/94.2
1/3	2/3	72.9/71.1	97.9/95.5	56.7/55.2	91.5/89.0	63.3/60.0	94.8/93.7
1/2	1/3	75.4/75.0	99.1/98.4	63.9/63.7	95.2/94.1	69.6/67.5	97.6/97.3
1/2	2/3	75.4/75.6	99.1/97.3	64.5/65.1	95.2/93.5	69.5/69.9	97.5/96.3
2/3	1/3	72.9/73.5	97.9/97.5	69.5/72.6	98.0/97.7	72.4/70.4	98.6/98.4
2/3	1/2	75.4/74.4	99.1/97.8	70.3/69.1	98.5/98.5	73.9/76.6	99.2/98.4
2/3	2/3	75.5/75.1	99.4/99.2	69.5/72.1	98.0/96.6	73.2/76.0	99.0/97.6

For the 'near open' case, $\phi = 1/(1 + ((k_2^{-1/2} + (1 - k_1)^{-1/2} + (1 - k_2)^{-1/2})/k_1^{-1/2})^{1/2})$. When $k_1 = 1/3$, $k_2 = 1/2$ (Fig. 6(c)), initially $C_3 > C_2$, because $f_{1,3} > f_{1,2}$ and $V_3 > V_2$; but later $C_3 < C_2$, because compartment 3 is flushed by a large amount of unexchanged fluid from compartment 4. When $k_1 = 1/2$, $k_2 = 2/3$ (Fig. 6(d)), $C_3 > C_2$. C_4 is the lowest because compartment 4 locates the furthest from the inlet. The agreement between the model predictions and the experimental results was quite good.

For the 'both open' case, $\phi = 1/(1 + ((k_2^{-1/2} + (1 - k_1)^{-1/2})/k_1^{-1/2})^{1/2})$. $C_1 > C_3 > C_2 > C_4$. When $k_1 = 1/2$, $k_2 = 2/3$ (Fig. 6(e)), the underestimation of C_4 was caused by the assumption that $f_{3,4} = 0$. In fact, $p_3 > p_4$, so C_4 increased faster than expected because $f_{3,4} > 0$. The experimental result was consistent with the model prediction when $k_1 = k_2 = 2/3$ (Fig. 6(f)).

The capacitance of the four node network is characterised by two variables (k_1, k_2). Table 3 summarises the theoretical and experimental flushing efficiency for different divisions of compartment volume. For the 'far open' case, k_1 and k_2 are symmetrical. At any fixed k_1 and k_2, the flushing efficiency at $T = 1$ or 3 is that 'far open'>'both open'>'near open'. This is because when the outlet is far from the inlet, there exists more chance for the incoming fluid to mix with and flush out the original fluid. The discrepancy between

Table 4. Dimensions of the hopper side and upper wing tank.

Compartment	Length (m)	Width (m)	Height (m)	Volume (m^3)
Bottom	27	3.3	1.4	11.5
Hopper side	27	1.9	5.0	17.4
Top wing	27	5.2	4.7	41.4

the experiment and the theory is within $\pm 3.3\%$ for $\bar{C}|_{T=1}$, and within $\pm 2.5\%$ for $\bar{C}|_{T=3}$, which proves the accuracy of the theory in assessing the flushed efficiency in the network.

The model predictions agree with measurements for the flux constrained cases. For the pressure constrained cases, the flow is sensitive to bypassing (due to the difficulty of maintaining the same pressure of the two exits). However, the discrepancy for the average flushing efficiency of the tank is small at three exchange volumes because the compartments which are not accurately predicted are always small in volume and do not contribute a lot to the average flushing efficiency of the whole tank.

4. Flushing from open-loop ballast tanks

In this section, the multizone model is applied to analyse the water flushing in two typical ballast tanks: a hopper side and upper wing tank and a 'J'-type bottom and side tank, shown in Fig. 7(a) and (b), respectively. The geometry is changed to guide ballast tank design and the exchange volumes required are estimated to meet the 95% reduction.

4.1. Model application

4.1.1. Flushing a hopper side and upper wing tank

A typical hopper side and upper wing tank typical of a bulk carrier is drawn in Fig. 7(a), which consists of 10 double bottom compartments, 10 hopper side compartments and 10 top wing compartments. The dimensions of the tank are shown in Table 4. Two 0.2 m diameter pipes connect the hopper side tanks to the top wing tanks. The incoming water is pumped into the corner bottom compartment and exits from two top wing compartments. There are 4, 2 and 1 holes between compartments within the bottom, the
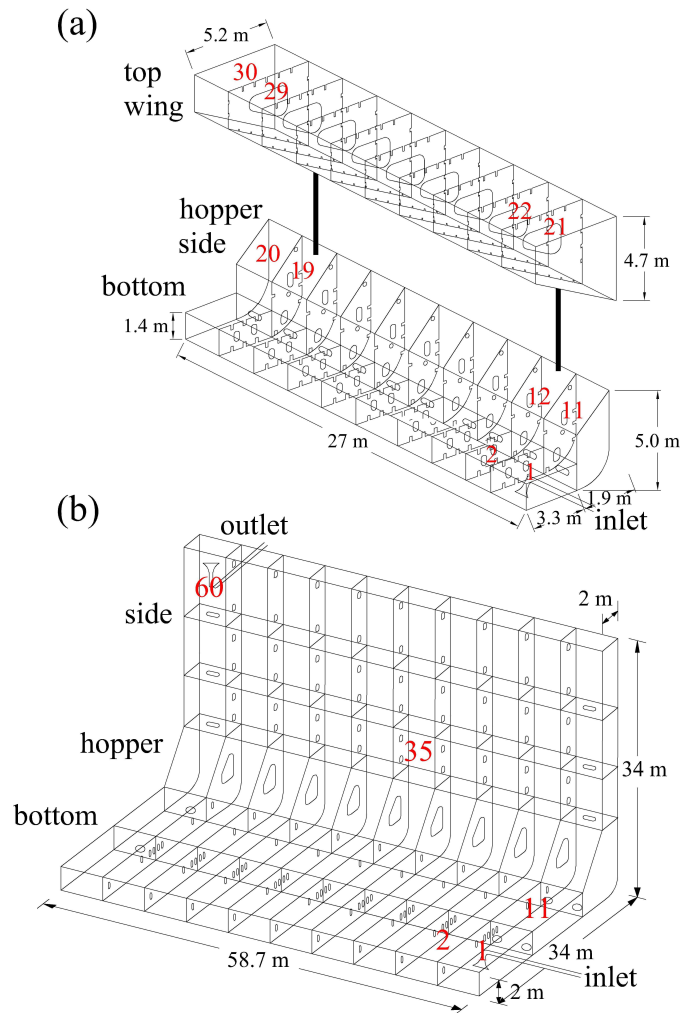
Fig. 7. Drawing of (a) a hopper side and upper wing tank (redrawn from Wilson et al. (2006)) and (b) a 'J'-type bottom and side tank (redrawn from American Bureau of Shipping (2004)) with internal structure. The compartments mentioned in the text are labelled with red numbers.

19

hopper side, and the top, respectively; and there is 1 hole connecting a double bottom compartment to a hopper side compartment. Usually both outlets are kept open during the flushing, but there is little flow between compartments of the top.

Fig. 8(a) shows the variation of $\bar{C}$ with time, respectively. For the 'both open' case, $\bar{C}$ increases between the displacement and the perfect mixing mode initially; at $T = 0.5 - 2.0$, $\bar{C}$ increases more slowly, below the perfect mixing mode; after $T = 2$, $\bar{C}$ is almost steady. The top wing compartments except 22 and 29 are hardly flushed, leading to a flushing efficiency of 73.3% at $T = 3$. Therefore, this outlet setting needs to be changed for a more effective flushing. In an earlier work, Kent and Parsons (2004) suggested that care is needed in detailed tank design to ensure complete exchange by the flow-through method. The setting and position of the outlet and the position of the connection pipes can be altered to improve the flushing efficiency. Firstly the outlet in compartment 22 is closed, and only the far outlet is kept open. In this case, there exists flow rates from compartment 22 to 29. The performance of $\bar{C}$ is much better than the that of the 'both open' case, which rises between the displacement and the perfect mixing mode from initially to $T = 2.7$ (see Fig. 8(b)). It does not achieve 95% because the two corner compartments 21 and 30 are not flushed. If the far outlet is further moved from compartment 29 to 30, compartment 30 can be flushed. In this case, $\bar{C}$ is over 95% after $T = 1.9$ (see Fig. 8(c)). Finally, the position of the two connection pipes is further moved to improve the flushing. When compartment 12 is connected to 22, compartment 31 cannot be effectively flushed, so the pipe is moved from between compartments 12 and 22 to between 11 and 21. To form a symmetrical structure, the pipe is also moved from between compartments 19 and 29 to between 20 and 30. In this case, all compartments are flushed efficiently. From Fig. 8(d), $\bar{C}$ is over 95% at $T = 1.8$, and 99.8% at $T = 3$. This finding is consistent with the CFD result of Kent and Parsons (2004) that the dual-trunk, single-port design gives the best flushing performance for the hopper side/upper wing tank, where $\bar{C} = 99.9\%$ at $T = 3$.

4.1.2. Flushing from a 'J'-type bottom and side tank

Fig. 7(b) shows the geometry of a 'J'-type bottom and side tank (typical of container vessels) with a volume of 14,267 m^3, which is 58.7 m long, 34 m wide and 34 m high, consisting of 20 double bottom compartments, 10 hopper compartments, and 30 side compartments. In this example, there are 9
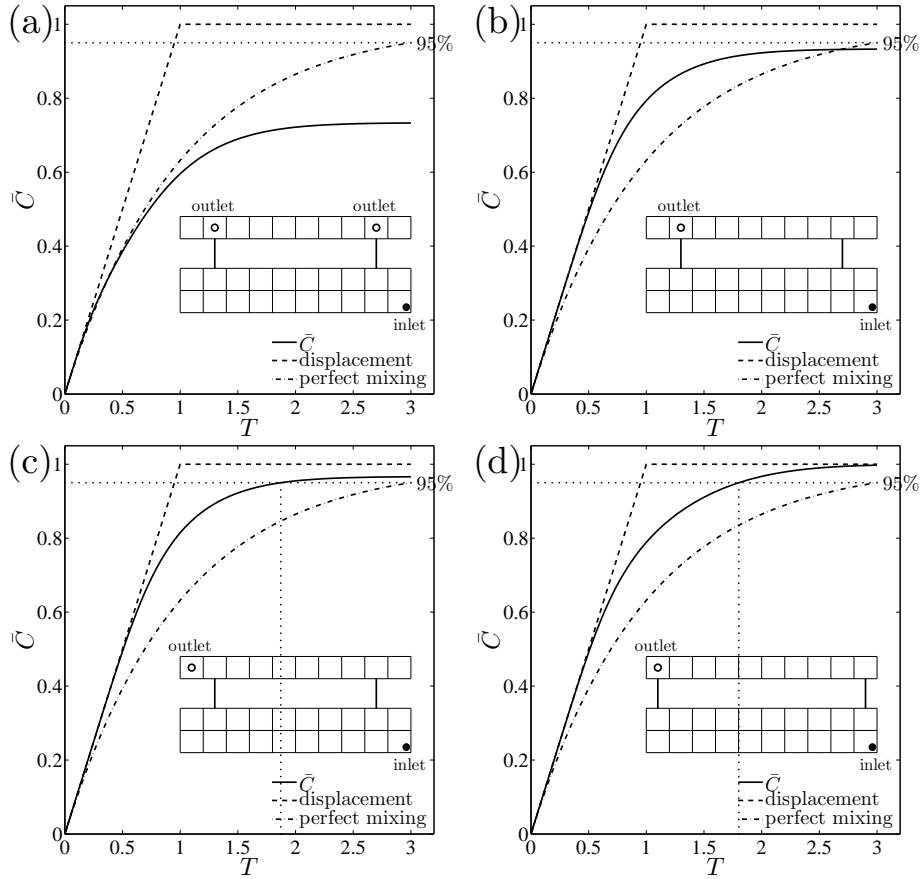
Fig. 8. Variation of $\bar{C}$ in the hopper side and upper wing tank, in comparison with the displacement and perfect mixing mode. The figures correspond to (a) the 'both open' case, (b) the 'far open' case, (c) the 'far open' case with revised outlet position and (d) the 'far open' case with revised position of the outlet and connection pipes.

21

transverse frames with 5.87 m spacing between the transverse bulkheads, and 14 ballast vent holes of 0.8 m × 0.6 m on each frame. The polygon manhole adjacent to the turn of the bilge has an area of 7.52 m². Three stringers are located at 9.6 m, 16.6 m and 24.6 m above the base line, respectively. On each stringer, there are 2 access holes of 0.75 m × 1.8 m, one located at the aft end and the other at the forward end. Between transverse frames on each stringer, there are 4 drain holes of 0.02 m × 0.24 m with 1.468 m of spacing at the sides of the longitudinal inner skin bulkhead and side shell plating. There is a side girder located 13 m off the centreline, and another side girder under the longitudinal bulkhead located 25.35 m off the centreline. On each side girder, there is an access manhole of 0.2 m × 0.8 m at the aft end and two of 1.0 m × 0.8 m at the forward end.

In this example, external water is pumped into the compartment on the right bottom and exits from the left top. Fig. 9 shows the time evolution of the flushing efficiency field in the tank. The compartments of the 1st row and those of the right top are flushed relatively faster. After one exchange volume, most of the initial fluid remains in the compartments on the left middle of the tank. At $T = 2$, almost all compartments have been flushed. This flushing efficiency is 99.9% at three exchange volumes, which agrees with the CFD result of Kent and Parsons (2004) that the three volumes pumping-through method for the 'J'-type tank can achieve a flushing efficiency of 99.7% when a single outlet is open. Figure 10(a) shows the variation of the tank flushing efficiency $\bar{C}$, C_{35} and C_{60} in time. Compartment 35 is a middle side compartment and compartment 60 is the outlet compartment (see Fig. 7(b)). The performance of $\bar{C}$ is much better than the perfect mixing mode. Initially, $\bar{C}$ follows the displacement rule until $T \simeq 0.5$, because the incoming fluid mixes sufficiently with the original fluid in the compartments close to the inlet, leading to little incoming fluid bypassing the tank. After three exchange volumes, the tank flushing efficiency is close to 100%. For $T \geq 1.7$, the flushing efficiency of the whole tank is over 95%. This means that when this ballast tank has been flushed with 1.7 volumes of clean water, the flushing efficiency can meet the IMO exchange standard. The concentration reductions are different among compartments. At $T \geq 1.7$, the flushing efficiency in compartment 35 and 60 is 87% and 99%, respectively. This means that at three exchange volumes, the NIS concentration in the water collected from the discharge port has not been reduced by 95% compared to the initial water.
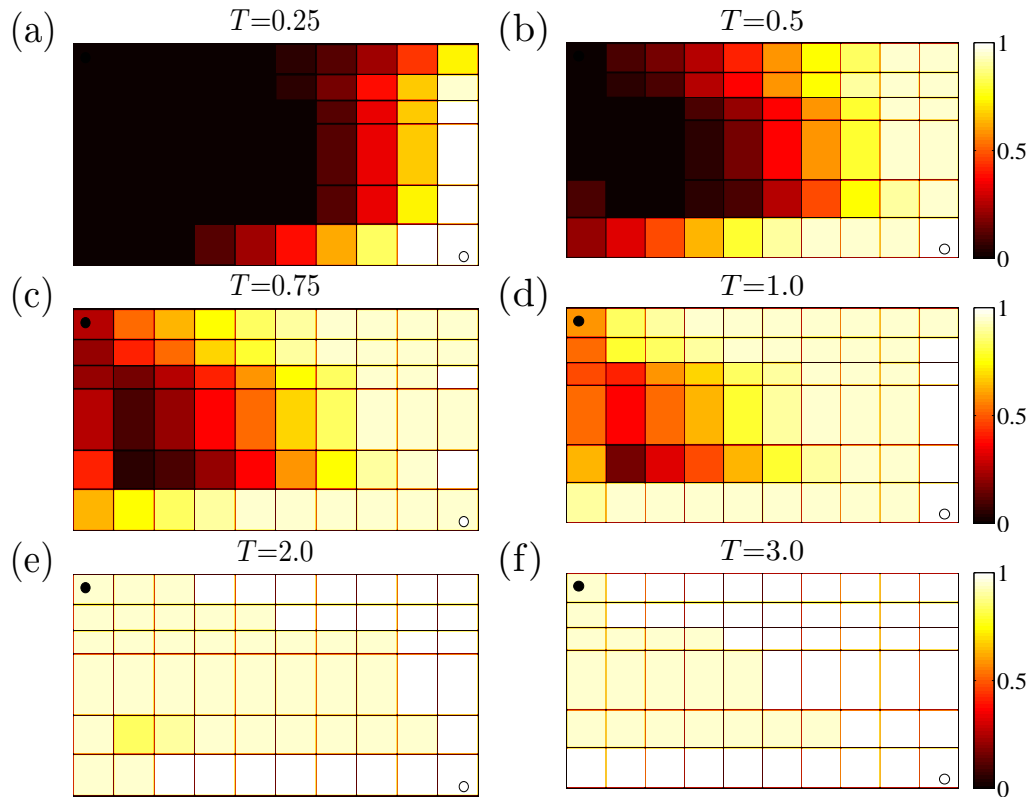
Fig. 9. Variation of the flushing efficiency field and the average flushing efficiency in the 'J'-type bottom and side tank at $T = 0.25 - 3.0$. The write and the black circles correspond to the inlet and the outlet, respectively.

4.2. Implications

In many cases, structural modification can improve the flushing efficiency in a ballast tank. Generally, it is useful to improve the flushing by setting a single outlet as far as possible from the inlet. To achieve an effective flushing, the position of the connection pipes should be adjusted to generate a flow system that can connect all compartments in the tank. In some cases, it is not necessary to flush three tank volumes of water to meet the 95% standard, and thus the running time of the ballast pumps can be reduced to save costs. The cost of ballast exchange is estimated at about \$0.23-0.32 per m^3 ballast water (adjusted for oil price increase from 2000 to 2014, see Gramling, 2000), so the cost saving of running the ballast pumps for a ship containing 4 considered 'J'-type tanks is about \$22,314-31,045 per stop when the flushing is reduced from 3 to 1.7 exchange volumes. A range of different sampling points would be expected on a ship (David, 2013), but the NIS reduction of these samples may be different when the flushing efficiency of the whole tank is 95%. When ballast water sampling is undertaken from the discharge port, the NIS reduction of the sample is not necessary to be 95% at three exchange volumes.

5. Flushing from a closed-loop ballast tank

5.1. Model application

In this section, the influence of treatment efficiency on the NIS removal rate of the future ballast system is studied. Considering the possibility of introducing new species from the sea or deep ocean to ballast tanks, scientists have provided a hybrid ballast water treatment system combined of an exchange unit and a treatment unit, within which water is circulated. In this system, the ballast tank is filled with port water, and during the voyage, the ballast water is continuously treated by the treatment unit and pumped back to the tank, where a circulation forms. In this case, the NIS removal rate depends on both the treatment efficiency (η) and the exchange volumes (T). When the water exchange in a single tank follows the perfect mixing rule, the NIS removal rate, R, increases as $1 - \exp(-\eta T)$. In reality, η can be 30-100% (see Table 1). This indicates that at the same exchange volumes, the NIS removal rate of the hybrid treatment system is lower than that of the current open-loop system. The NIS removal rate of the above 'J'-type ballast tank with a treatment unit, and the influence of the treatment efficiency and exchange volumes on it will be discussed.
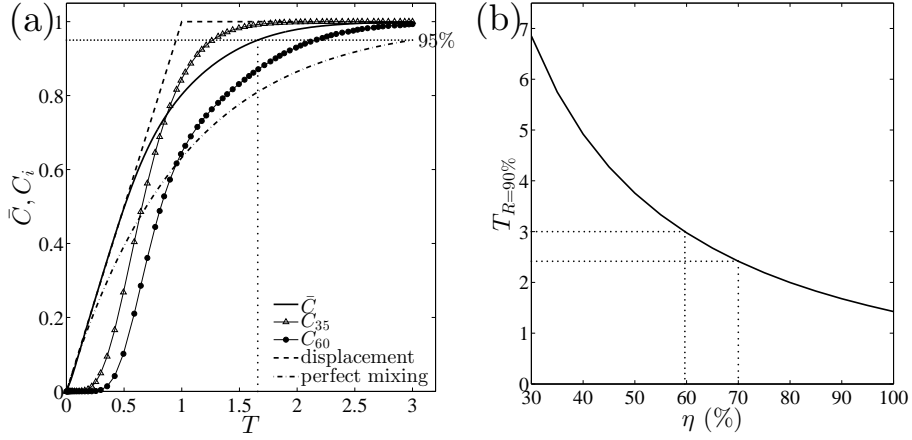
Fig. 10. Flushing from a 'J'-type bottom and side tank. (a) shows the variation of $\bar{C}$, C_{35} and C_{60} against exchange volumes, compared with the displacement and perfect mixing mode. The dotted line showing $\bar{C} = 95\%$ is the IMO exchange requirement. (b) shows the exchange volumes required to achieve 90% NIS removal rate against the treatment efficiency (η).

When applying the model to the closed-loop system, the flushing efficiency of the inlet compartment (compartment 1) is set as that of the outlet compartment (compartment 60) improved by the treatment unit. For example, for the 'J'-type tank with a treatment unit, C_1 varies as

$$\frac{\mathrm{d}C_1}{\mathrm{d}T} = \frac{V}{V_1}(Q(C_{60} + \eta(1 - C_{60})) - f_{1,2}C_1 - f_{1,11}C_1), \qquad (8)$$

where C_60 is the flushing efficiency of the outlet compartment, 2 and 11 are compartments connected to compartment 1. The mass flux of the backflow to compartment 1 is $Q(C_{60} + \eta(1 - C_{60}))$. Fig. 10(b) shows the exchange volumes required to achieve the NIS removal rate of 90% against the treatment efficiency (η). It can be seen that the lower the treatment efficiency is, the longer time is needed to achieve the required NIS removal rate. The treatment efficiency needs to be at least 59% to achieve the 90% NIS removal rate at three exchange volumes. At a treatment efficiency of $\eta = 70\%$, 2.4 times circulation is required to achieve a NIS removal rate of 90%.

25

5.2. Implications

In the hybrid ballast water treatment system, the NIS removal rate depends on both the flushing efficiency and the treatment efficiency. For the 'J'-type bottom and side tank considered, when the treatment efficiency is less than 59%, more than three exchange volumes is needed to attain the 90% NIS removal rate, so it is recommended to employ only the ballast water flushing technology to satisfy the IMO exchange standard if permitted. When the treatment efficiency is greater than 59%, the exchange volumes required for the NIS in the tank to be reduced to 10% of the initial concentration are less than three.

6. Conclusion

The NIS removal rate in a multi-compartment ballast tank depends on the geometry (hole resistance, compartment capacitance, outlet position and connection pipes position), exchange volumes (flushing time) and treatment technology. To analyse the influence of geometry of an open/closed-loop tank, a multizone model is developed and validated. The model predictions agree extremely well with the measurements when the flow is constrained by volume flux. When there were two exits and controlled by the pressure being the same at the two outlets, experimentally the results are sensitive to the arrangement when the resistance is strongly inhomogeneous.

For a hopper side and upper wing tank, change of structure may significantly increase the flushing efficiency. Setting a single outlet far from the inlet may improve the flushing efficiency to over 95% at three exchange volumes. For the 'J'-type bottom and side tank considered, configurations are identified where the requirement for exchange volumes can be relaxed. The reduction of flushing from 3 to 1.7 exchange volumes may achieve a cost saving of about $22,314-31,045 for a ship per stop. When ballast water sampling is undertaken from the discharge port, the NIS reduction of the sample is not necessary to be 95% at three exchange volumes.

For the future closed-loop treatment system consisting of an exchange unit and a treatment unit, at a treatment efficiency of 70%, 2.4 times circulation is needed to achieve the 90% NIS removal rate; the treatment technology for the 'J'-type tank needs to achieve at least 59% efficient to attain a 90% NIS removal rate at three exchange volumes.

Acknowledgement

Appendix A. Mathematical model of a four node network

The flow in the four node network is determined by 4 mass conservation equations and 4 pressure loss equations. To simplify the notation, ϕ is defined as $f_{1,2}/Q$, thus

$$f_{1,3} = (1 - \phi)Q, \quad f_{2,4} = \phi Q, \quad Q_{3,\text{out}} = (1 - \phi)Q - f_{3,4}, \quad Q_{4,\text{out}} = \phi Q + f_{3,4}; \tag{A.1}$$

$$
\begin{aligned}
p_1 - p_2 &= \psi_{1,2}\rho|f_{1,2}|f_{1,2}, & p_3 - p_4 &= \psi_{3,4}\rho|f_{3,4}|f_{3,4}, \\
p_1 - p_3 &= \psi_{1,3}\rho|f_{1,3}|f_{1,3}, & p_2 - p_4 &= \psi_{2,4}\rho|f_{2,4}|f_{2,4},
\end{aligned} \tag{A.2}
$$

where $\psi_{i,j} = \zeta_{i,j}A_{i,j}{}^{-2}$. For different outlet arrangements, the expressions for the flow rates are shown in Table A1. The flushing efficiency in each compartment evolves according to

$$
\begin{aligned}
\frac{\mathrm{d}C_1}{\mathrm{d}T} &= \frac{1}{k_1 k_2}\left(S - C_1\right), \\
\frac{\mathrm{d}C_2}{\mathrm{d}T} &= \frac{1}{(1 - k_1)k_2}\left(\phi C_1 - \phi C_2\right), \\
\frac{\mathrm{d}C_3}{\mathrm{d}T} &= \frac{1}{k_1(1 - k_2)}\left((1 - \phi)C_1 - \frac{f_{3,4}}{Q}(H(f_{3,4})C_3 + H(-f_{3,4})C_4) - \frac{Q_{3,\text{out}}}{Q}C_3\right), \\
\frac{\mathrm{d}C_4}{\mathrm{d}T} &= \frac{1}{(1 - k_1)(1 - k_2)}\left(\phi C_2 + \frac{f_{3,4}}{Q}(H(f_{3,4})C_3 + H(-f_{3,4})C_4) - \frac{Q_{4,\text{out}}}{Q}C_4\right).
\end{aligned} \tag{A.3}
$$

The test case considered, to validate the time dependence of C, is one where the system is initially devoid of a contaminant, which is introduced through the inlet. This test is described by the initial condition, $C_i|_{T=0} = 0$, and a source term $S = 1$. The Heaviside function (where $H(X) = 1$ for $X \geq 0$ and $H(X) = 0$ for $X < 0$) is needed to prevent flow in the wrong direction. For the four node network, where the flux between each compartment is known, C_i can be explicitly determined from (A.3) for the case of $k_1 = k_2 = 1/2$.

27

Table A1. Expressions of flow rates when $k_1 = k_2 = 1/2$ in the four node inhomogeneous network.

| | Flux constrained | | Pressure constrained |
	Far open	Near open	Both open
ϕ	$\dfrac{1}{1+\left(\frac{\psi_{1,2}+\psi_{2,4}}{\psi_{1,3}+\psi_{3,4}}\right)^{\frac{1}{2}}}$	$\dfrac{1}{1+\left(\frac{\psi_{1,2}+\psi_{2,4}+\psi_{3,4}}{\psi_{1,3}}\right)^{\frac{1}{2}}}$	$\dfrac{1}{1+\left(\frac{\psi_{1,2}+\psi_{2,4}}{\psi_{1,3}}\right)^{\frac{1}{2}}}$
Flux constraint	$Q_{3,\text{out}} = 0,$ $Q_{4,\text{out}} = Q$	$Q_{3,\text{out}} = Q,$ $Q_{4,\text{out}} = 0$	$Q_{3,\text{out}} = (1-\phi)Q,$ $Q_{4,\text{out}} = \phi Q$
Pressure constraint	$p_4 = 0$	$p_3 = 0$	$p_3 = p_4 = 0$

If all the compartments of the network are identical, i.e. $k_1 = k_2 = 1/2$, τ is defined as

$$\tau = \frac{Qt}{V_i}. \tag{A.4}$$

For the 'far open' case, the solution is

$$C_1 = 1 - e^{-\tau},$$

$$C_2 = 1 - \frac{1}{1-\phi}e^{-\phi\tau} + \frac{\phi}{1-\phi}e^{-\tau},$$

$$C_3 = 1 - \frac{1}{\phi}e^{-(1-\phi)\tau} + \frac{1-\phi}{\phi}e^{-\tau},$$

$$C_4 = 1 - \frac{\phi}{(1-\phi)^2}e^{-\phi\tau} - \frac{1-\phi}{\phi^2}e^{-(1-\phi)\tau}$$

$$+ \left(\left(\frac{1}{\phi(1-\phi)} - 3\right)\tau + \frac{1}{\phi^2(1-\phi)^2} - \frac{3}{\phi(1-\phi)} - 1\right)e^{-\tau}; \tag{A.5}$$

for the 'near open' case, the solution is

$$
\begin{aligned}
C_1 =&\, 1 - e^{-\tau}, \\
C_2 =&\, 1 - \frac{1}{1-\phi}e^{-\phi\tau} + \frac{\phi}{1-\phi}e^{-\tau}, \\
C_3 =&\, 1 - \left(\frac{\phi^2}{(1-\phi)^2}\tau - \frac{3\phi^2-\phi}{(1-\phi)^3}\right)e^{-\phi\tau} \\
& - \left(\frac{3\phi^2-3\phi+1}{(1-\phi)^2}\tau - \frac{\phi^3-6\phi^2+4\phi-1}{(1-\phi)^3}\right)e^{-\tau}, \\
C_4 =&\, 1 - \left(\frac{\phi}{1-\phi}\tau - \frac{2\phi-1}{(1-\phi)^2}\right)e^{-\phi\tau} - \frac{\phi^2}{(1-\phi)^2}e^{-\tau};
\end{aligned}
\tag{A.6}
$$

for the 'both open' case, the solution is

$$
\begin{aligned}
C_1 =&\, 1 - e^{-\tau}, \\
C_2 =&\, 1 - \frac{1}{1-\phi}e^{-\phi\tau} + \frac{\phi}{1-\phi}e^{-\tau}, \\
C_3 =&\, 1 - \frac{1}{\phi}e^{-(1-\phi)\tau} + \frac{1-\phi}{\phi}e^{-\tau}, \\
C_4 =&\, 1 - \left(\frac{\phi}{1-\phi}\tau - \frac{2\phi-1}{(1-\phi)^2}\right)e^{-\phi\tau} - \frac{\phi^2}{(1-\phi)^2}e^{-\tau}.
\end{aligned}
\tag{A.7}
$$

References

American Bureau of Shipping, 2004. Inert gas system for ballast tanks.

Cenedese, C., Dalziel, S. B., 1998. Concentration and depth field determined by the light transmitted through a dyed solution. In: 8th International Symposium on Flow Visualization. pp. 1–5.

Champ, M. A., 2002. Marine testing board for certification of ballast water treatment technologies. Mar. Pollut. Bull. 44, 1327–1335.

Chen, J., Huo, J. Z., Zhang, Y., Zhang, D. Y., Zhang, W. Y., Lin, Y., 2013. Heuristic solution strategy for the sequential ballast water exchange problem. J. Waterw. Port C. Div. 139 (1), 72–80.

Chen, Q. Y., 2009. Ventilation performance prediction for buildings: a method overview and recent applications. Build. Environ. 44, 848–858.

Chen, Q. Y., Lee, K., Mazumdar, S., Poussou, S., Wang, L. Z., Wang, M., Zhang, Z., 2010. Ventilation performance prediction for buildings: model assessment. Build. Environ. 45 (2), 295–303.

Chu, C. R., Chiu, Y. H., Wang, Y. W., 2010. An experimental study of wind-driven cross ventilation in partitioned buildings. Energ. Buildings 42 (5), 667–673.

Chu, C. R., Wang, Y. W., 2010. The loss factors of building openings for wind-driven ventilation. Build. Environ. 45, 2273–2279.

David, M., 2013. Ballast water sampling for compliance monitoring - ratification of the Ballast Water Management Convention. Tech. rep., Final report of research study for WWF International. 66 pp.

Eames, I., Landeryou, M., Greig, A., Snellings, J., 2008. Continuous flushing of contaminants from ballast water tanks. Mar. Pollut. Bull. 56 (2), 250–260.

Endresen, Ø., Behrens, H. L., Brynestad, S., Andersen, A. B., Skjong, R., 2004. Challenges in global ballast water management. Mar. Pollut. Bull. 48 (7-8), 615–623.

Feustel, H., Smith, B. V., 1997. COMIS 3.0 - User s guide. Berkeley, CA: Lawrence Berkeley National Laboratory.

Flagella, M. M., Verlaque, M., Soria, A., Buia, M. C., 2007. Macroalgal survival in ballast water tanks. Mar. Pollut. Bull. 54, 1395–1401.

Gavand, M. R., McClintock, J. M., Amsler, C. D., Peters, R. W., Angus, R. A., 2007. Effects of sonication and advanced chemical oxidants on the unicellular green alga *Dunaliella tertiolecta* and cysts, larvae and adults of the brine shrimp *Artemia salina*: a prospective treatment to eradicate invasive organisms from ballast water. Mar. Pollut. Bull. 54, 1777–1788.

Goncalves, A. A., Gagnon, G. A., 2012. Recent technologies for ballast water treatment. Ozone-Sci. Eng. 34 (3), 174–195.

Gramling, J, 2000. Ballast water and shipping patterns in Puget Sound - considerations for siting of alternative ballast water exchange zones. Tech. rep., Puget Sound Water Quality Action Team, Olympia, Washington.

Heiselberg, P., Svidt, K., Nielsen, P. V., 2001. Characteristics of airflow from open windows. Build. Environ. 36, 859–869.

International Maritime Organization, 2004. International convention for the control and management of ships ballast water and sediments. Int. Conf. on Ballast Water Management for Ships, London.

International Maritime Organization, Oct. 2008. Guidelines for approval of ballast water management systems (G8).

Kent, C. P., Parsons, M. G., 2004. Computational fluid dynamics study of the effectiveness of flow-through ballast exchange. Trans. SNAME 112, 241–270.

King, D. M., Hagan, P. T., Riggio, M., Wright, D. A., 2012. Preview of global ballast water treatment markets. J. Mar. Eng. Technol. 11 (1), 3–16.

Li, M., Wu, C. L., Zhao, S. Q., Yang, Y., 2008. State-space model for airborne particles in multizone indoor environments. Atmos. Environ. 42, 5340–5349.

Mamlook, R., Badran, O., Abu-Khader, M. M., Holdo, A., Dales, J., Dec. 2007. Fuzzy sets analysis for ballast water treatment systems: best available control technology. Clean Technol. Envir. 10 (4), 397–407.

Meizig, H. D., Schmidt, P. K., 1965. Pressure distribution during parachute opening. Tech. rep., Deutsche Forschungsanstalt fuer Luft- und Raumfahrt E V Brunswick (West Germany) Institut fuer Flugmechanik.

Montalbano, M., 1962. Tables, flow-charts, and program logic. IBM Systems Journal 1, 51–63.

Murphy, K., Boehme, J., Coble, P., Cullen, J., Field, P., Moore, W., Perry, E., Sherrell, R., Ruiz, G., 2004. Verification of mid-ocean ballast water exchange using naturally occurring coastal tracers. Mar. Pollut. Bull. 48 (7), 711–730.

Parker, S., Bowman, V., 2011. State-space methods for calculating concentration dynamics in multizone buildings. Build. Environ. 46, 1567–1577.

Parsons, M. G., Harkins, R. W., 2000. The Great Lakes Ballast Technology Demonstration Project filtration mechanical test program. Mar. Technol. 37, 129–140.

Perakis, A. N., Yang, Z. Y., Jan. 2003. Options for nonindigenous species control and their economic impact on the Great Lakes and St. Lawrence seaway: a survey. Mar. Technol. Sname N. 40 (1), 34–41.

Qi, Z., Eames, I., Greig, A., 2014. Flushing ballast tanks. Ocean Eng. 89, 157–172.

Tsolaki, E., Diamadopoulos, E., Jan. 2010. Technologies for ballast water treatment: a review. J. Chem. Technol. Biot. 85 (1), 19–32.

Waite, T. D., Kazumi, J., Lane, P. V. Z., Farmer, L. L., Smith, S. G., Smith, S. L., Hitchcock, G., Capo, T. R., 2003. Removal of natural populations of marine plankton by a large-scale ballast water treatment system. Mar. Ecol. - Prog. Ser. 258, 51–63.

Wilson, W., Chang, P., Verosto, S., Atsavapranee, P., Reid, D. F., Jenkins, P. T., 2006. Computational and experimental analysis of ballast water exchange. Nav. Eng. J. 118 (3), 25–36.

Zhao, Y., Yoshino, H., Okuyama, H., 1998. Evaluation of the COMIS model by comparing simulation and measurement of airflow and pollutant concentration. Indoor Air 8, 123–130.